MACH WAVE EMISSION IN A PLANE SUPERSONIC JET AT HIGH CONVECTIVE MACH NUMBERS

Daisuke Watanabe , Hiroshi Maekawa
Graduate School of Engineering, Hiroshima University

Keywords: *Supersonic jet, Transition, Turbulence, Mach wave, DNS*

Abstract

The three-dimensional time dependent compressible Navier-Stokes equations are numerically solved to study acoustic emission mechanism in a supersonic plane jet at high convective Mach numbers using high-order compact upwind schemes. High-order compact schemes of 5th order developed by Deng and Maekawa (1996, 1997)[1][2] are used for spatial derivatives and a 4th order Runge-Kutta scheme is employed for time advancement. Navier-Stokes characteristic boundary conditions are used in the streamwise and vertical direction and periodic boundary conditions in the spanwise directions. Numerical results for the convective Mach number $Mc = 1.17$ are presented (Mc is defined by eq.(16) in Section 2). Two different cases were investigated. The first case is the jet forced by the linear unstable modes. The second case is the jet flow forced randomly.

The numerical results provide new physical insights into three-dimensional structures of a plane jet. Upstream disturbance conditions play an important role for the evolution of the downstream structure, such as development of shear layers and transition process in a jet. Growth of 3D-A1 mode is responsible for the Λ structure in a plane jet. The 2-D A1 mode, whose phase velocity is larger than the ambient speed of sound, is responsible for the Mach waves emission. The growth and decay of the supersonic phase 2-D A1 mode link to the intense sound radiation in the 3D DNS.

1 Introduction

Compressible jets, which can be found in many applications such as rocket, scramjet, ramjet and turbojet engines, have been of fundamental importance in the study of compressible free shear flows. With new noise regulations, reducing of acoustic noise is the one of key technological challenges facing proposed supersonic commercial aircraft. The numerical investigation of supersonic jets is expected to guide such technological progress on aircraft where the jet exhaust velocity is supersonic. As Seiner (1992) [3] points out in his article, methods have long been sought to find an efficient means for reduction of jet noise either active or passive turbulence control measures. Progress in this area has been limited by unclear understanding of the physical supersonic jet noise source mechanism. These mechanisms have been extensively studied using round jets. While non-round jet exit geometry has been experimentally proved to provide beneficial noise reduction relative to round jets. Mach wave emission and shock noise are the dominant acoustic sources of supersonic jet noise. Improperly expanded nozzles produce shock noise that dominates acoustic emission in the jet forward quadrant. Shock noise, however, could be minimized through appropriate design of nozzle geometry. It has been observed experimentally that the acoustic radiation from jets is dominated by Mach waves (see review by Tam 1995 [4]). Turbulent structures traveling at supersonic speed within the jet are generally thought to be responsible for Mach waves, and they have been

modeled as linear stability modes. Reduction of Mach wave emission represents the most serious challenge to the successful design of a suppressor nozzle. The understanding of jet turbulence and noise emission is very crucial for jet investigations. DNS of supersonic round jet was performed and brought much light to these mechanisms. Freund *et al.* (2000) [5] simulated a perfectly expanded Mach 1.92 jet at $Re_D = 2000$ based on the jet nozzle diameter and its sound field. For non-round jet exit geometry, Stanley, Sarkar and Mellado(2002) [6] carried out there-dimensional direct numerical simulation for compressible plane jet for $Mc = 0.16$ and $Re_h = 3000$ based on the jet nozzle width.

Watanabe and Maekawa [7] performed linear stability analysis and three-dimensional temporal direct numerical simulation for high-convective Mach number plane jet. Their linear stability analysis showed that the high wave number 2-D antisymmetirc mode phase velocity was larger than the ambient sound speed for high-convective Mach numbers larger than 1. On the other hand, the phase velocity of 3-D antisymmetirc mode near maximum unstable was always smaller than the ambient sound speed for investigated convective Mach number range (Mc<1.55). They described that radiating unstable modes, such as 2-D antisymmetirc mode, were important for acoustic emission for high Mach number jets. In addition, a comparison of 3D and 2D DNS results showed that acoustic energy represented by dilatation fields of averaged div **u** grows and decays when the potential core of the jet collapsed due to 3-D antisymmetric mode growth.

We investigate, by means of DNS, the spatially development of high Mach number plane jet forced with the unstable/random disturbances. Both the fluid dynamic structures and noise of plane jets are studied. In the present study, we focus on the effect of inflow disturbances on the transition of the plane jet using spatial 3-D DNS and linear stability analysis. The plane jet is of interest, as described above, due to practical importance of supersonic combustion and jet noise generation. The nonlinear structures resultant from a couple of linear unstable modes at high convective Mach numbers and sound fields correlated to the energy evolution of various modes in the nonlinear process are examined.

2 Computational Details

In the direct numerical simulations, the nondimensional equations governing the conservation of mass, momentum, and energy for a compressible Newtonian fluid are solved using fifth-order dissipative compact finite difference schemes [1] in all directions. On a uniform grid, the fifth-order dissipative compact approximations for the first derivatives are expressed in the following form

$$\begin{aligned}\frac{1}{3}(1-\alpha_d)u'_{j-1}+u'_j+\frac{1}{3}(1+\alpha_d)u'_{j+1} &= \frac{1}{36h}(u_{j+2}-u_{j-2})+\frac{7}{9h}(u_{j+1}-u_{j-1})\\ &+\frac{1}{18h}\alpha_d(u_{j+2}-2u_j+u_{j-2})\\ &+\frac{4}{9h}\alpha_d(u_{j+1}-2u_j+u_{j-1}),\end{aligned} \tag{1}$$

where α_d is a control parameter of dissipative and dispersive error and here $\alpha_d = \pm 0.25$. In this scheme, $\alpha_d = 0$ corresponds to Lele's sixth-order central compact scheme [8]. To apply this scheme to the following nonlinear system,

$$\frac{\partial \mathbf{Q}}{\partial t}+\frac{\partial \mathbf{F}}{\partial x} = \textit{viscous term}, \tag{2}$$

where $\mathbf{Q}$ and $\mathbf{F}$ are

$$\mathbf{Q}=\begin{pmatrix}\rho\\ \rho u_1\\ E_T\end{pmatrix},\quad \mathbf{F}=\begin{pmatrix}\rho u_1\\ \rho u_1 u_1+p\\ (E_T+p)u_1\end{pmatrix}, \tag{3}$$

a local Lax-Friedrichs scheme could be used to split an invisid flux vector $\mathbf{F}$ into positive and negative wave fields so that the upwind schemes could be applied,

$$\mathbf{F}=\mathbf{F}^+ + \mathbf{F}^-. \tag{4}$$

where

$$\begin{aligned}\mathbf{F}^+ &= \frac{1}{2}(\mathbf{F}+\lambda\mathbf{Q}),\\ \mathbf{F}^- &= \frac{1}{2}(\mathbf{F}-\lambda\mathbf{Q}),\end{aligned} \tag{5}$$

where λ is a positive parameter to decide numerical viscosity effectiveness. In this study, λ is 1.

The governing equations are given as follows;

$$\frac{\partial \rho}{\partial t} + \frac{\partial (\rho u_i)}{\partial x_i} = 0, \tag{6}$$

$$\frac{\partial (\rho u_i)}{\partial t} + \frac{\partial (\rho u_i u_j)}{\partial x_j} = -\frac{\partial p}{\partial x_i} + \frac{\partial \tau_{ij}}{\partial x_j}, \tag{7}$$

$$\frac{\partial E_T}{\partial t} + \frac{\partial (E_T u_j)}{\partial x_j} = - \frac{\partial (p u_j)}{\partial x_j} + \frac{\partial (u_i \tau_{ij})}{\partial x_j} - \frac{\partial q_j}{\partial x_j} \tag{8}$$

where

$$E_T = \frac{p}{(\gamma - 1)} + \frac{\rho u_i u_i}{2}, \tag{9}$$

$$q_j = -\frac{\mu}{(\gamma-1) M_\infty^2 Re Pr} \frac{\partial T}{\partial x_j}, \tag{10}$$

$$\tau_{ij} = \frac{\mu}{Re}\left[\left(\frac{\partial u_i}{\partial x_j} + \frac{\partial u_j}{\partial x_i}\right) - \frac{2}{3}\delta_{ij}\frac{\partial u_k}{\partial x_k}\right], \tag{11}$$

$$T = \frac{\gamma M_\infty^2 p}{\rho}, \tag{12}$$

$$\mu = T^{2/3}. \tag{13}$$

The all variables, in all the following discussions, are nondimensionalized by the characteristic physical scales such as $\bar{u}_{1j}, \rho_\infty, T_\infty$ and the jet nozzle half-width of b where the subscripts j and ∞ indicate the jet centerline and the ambient fluid, respectively. The flow field of a jet issuing from rectangular nozzle into an ambient fluid can be divided into a potential core region, a transition region, and a fully developed region. The "top-hat" jet profile belongs to the potential core region with a thin but finite shear layer.

We employed the mean velocity profile given by

$$\bar{u}_1(x_2) = \frac{\bar{u}_{1j}}{2}\left[1 - \tanh\left[\frac{12.5}{4}\left(\frac{x_2}{b} - \frac{b}{x_2}\right)\right]\right]. \tag{14}$$

The mean temperature was calculated with a Crocco-Busemann relation for unity Prandtl number;

$$\bar{T} = M_\infty^2 \frac{\gamma - 1}{2}\frac{(u_1 \bar{u}_{1j} - u_1^2)}{\bar{u}_{1j}} + \frac{\bar{T}_j u_1}{\bar{u}_{1j}} + \frac{\bar{T}_\infty (\bar{u}_{1j} - u_1)}{\bar{u}_{1j}}, \tag{15}$$

where γ is the ratio of specific heats. $M_\infty = \bar{u}_{1j}/c_\infty$ and c_∞ is the speed of sound at the quiescent stream. The jet centerline Mach number $M_j = \bar{u}_{1j}/c_j$ is obtained from the relation $M_j = M_\infty \times c_\infty / c_j$. The jet was heated with exit temperature ratio $T_j/T_\infty = 1.12$. This ratio was used for the simulation of a perfectly expanded Mach 1.92 jet [5]. A jet convective Mach number Mc may be defined by

$$Mc = \frac{M_j \sqrt{\bar{T}_j / \bar{T}_\infty}}{1 + \sqrt{\bar{T}_j / \bar{T}_\infty}}. \tag{16}$$

By using equation (16), the convective Mach number for the Mach 1.92 jet[5] is $Mc = 0.99$. The particular choices of convective Mach numbers were made in view of experience with planer, compressible shear layers indicating that at $Mc = 0.60$ and above, the most highly amplified disturbances are no longer two-dimensional but become three-dimensional. The lower and higher values of Mc are characteristic of nearly incompressible and highly compressible shear flows. The definition of convective Mach number is the same as related jet stability and DNS studies. Time advancement was performed by a fourth-order Runge-Kutta algorithm. For 3-D spatial DNS, the computational mesh was $N_{x_1} \times N_{x_2} \times N_{x_3} = 301 \times 201 \times 100$. Mesh points were compressed in the streamwise and normal direction. NSCBC (Navier-Stokes Characteristic

Boundary Conditions) [9] were implemented in the treatment of the boundaries at the in/outflow and far normal regions. Periodic boundary conditions were implemented in the spanwise directions. Outflow boundaries were located in $x_1 = 45b$ for streamwise and $x_2 = \pm 10b$ (see figure 1).

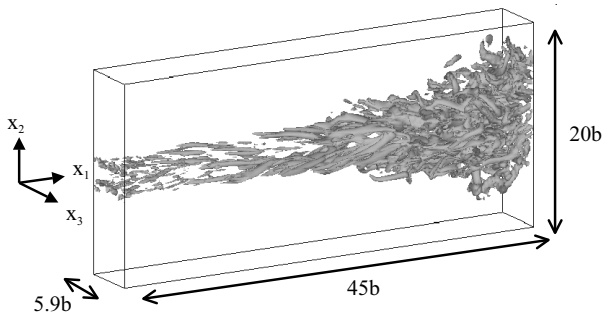

Fig. 1 computational box

3 Results

Two different types of forcing of the inlet for spatial DNS for $Mc = 1.17$ and $Re_b = 1000$, which corresponds to $Re_h = 2000$ based on the jet nozzle width h, are performed to investigate the flow structure and noise generation. The effects of the amplitude level of the perturbation are also investigated. In the first case, unstable eigenfunctions are used to perturb the jet (hereafter referred to as eigenfunction case). In the second case, disturbances of random phase are used (hereafter referred to as random case). Cases of E1 and E2 are the jets perturbed by linear eigenfunctions of the most unstable 2-D S2 wave and the 2-D A1 wave, together with eigenfunctions of a pair of oblique 3-D A1 waves of equal and opposite angle at the inlet. The inlet disturbance vector $\tilde{\mathbf{d}}$ can be written as

$$\begin{aligned}\tilde{\mathbf{d}} &= A_{\text{2-D A1}}\hat{\mathbf{d}}_{\text{2-D A1}}\exp[\mathrm{i}(-\omega_{\text{2-D A1}}t)] \\ &+ A_{\text{2-D S2}}\hat{\mathbf{d}}_{\text{2-D S2}}\exp[\mathrm{i}(-\omega_{\text{2-D S2}}t)] \\ &+ A_{\text{3-D A1}}\hat{\mathbf{d}}_{\text{3-D A1}}\exp[\mathrm{i}(\beta x_3 - \omega_{\text{3-D A1}}t)] \\ &+ A_{\text{3-D A1}}\hat{\mathbf{d}}_{\text{3-D A1}}\exp[\mathrm{i}(-\beta x_3 - \omega_{\text{3-D A1}}t)], \quad (17)\end{aligned}$$

where $\hat{\mathbf{d}}$ is the eigenfunction vector and A are the amplitudes of corresponding modes. For E1 case, $A_{\text{2-D A1}}$ and $A_{\text{2-D S2}}$ were 1% and $A_{\text{3-D A1}}$ was 0.5% of the jet velocity. For E2 case, all amplitudes of modes were set 1%. The spanwise wavenumber β was chosen to correspond to a pair of oblique waves inclined at $\theta = \pm 51^\circ$ relative to the streamwise direction. This choice in angle is attributable to the maximum growth rate of the 3-D mode. Cases of R1 and R2 are the jets forced with randomly chosen three-dimensional white noise. The root mean square of streamwise velocity component was 1% of the jet velocity for R1 case and was 3% for R2 case. In the all cases, the length of the computational domain in the spanwise directions, L_3, is determined from linear stability theory. Therefore, $L_3 = 2\pi/\beta$, where $\beta = 1.05$.

3.1 Jet structure

Figure 2 shows the downstream development of the vortical structure in the jet for E1 case. The structure is visualized with iso-surfaces of the second invariant Q of the velocity gradient tensor. At the locations of $0 < x_1 < 10b$, we can see the almost symmetric two-dimensional rolled up structures due to the growth of the 2-D S2 mode. Between the locations of 10b and 20b, alternative Λ-shaped structures appear downstream after the two-dimensional structures. The oblique mode (3-D A1)result in the Λ-shaped structures. After appearance of Λ-shaped structure, the jet structure spreads outside rapidly and the fully developed three-dimensional structures are generated inside the jet. In the transition regime, the fluid rises upstream associated with the Λ-shaped rollers. In Fig.2, it is difficult to see a large effect of 2-D A1 mode on the vortical structure.

The effects of the amplitude levels of the 3-D A1 mode on the jet shear layers expansions are investigated. Figures 3(a) and (b) show the contours of the mean streamwise velocity for E1 and E2 cases, respectively. Increase of the amplitude level of the 3-D A1 mode leads to sooner shear layers expansions. Figure 3(a) indicate that the shear layers spread rapidly around $x_1 = 20b$ for E1 case. For E2 case, as shown in Fig.3(b), the shear layers spread rapidly around $x_1 = 15b$. Around these points, as shown in Fig.2, the Λ-

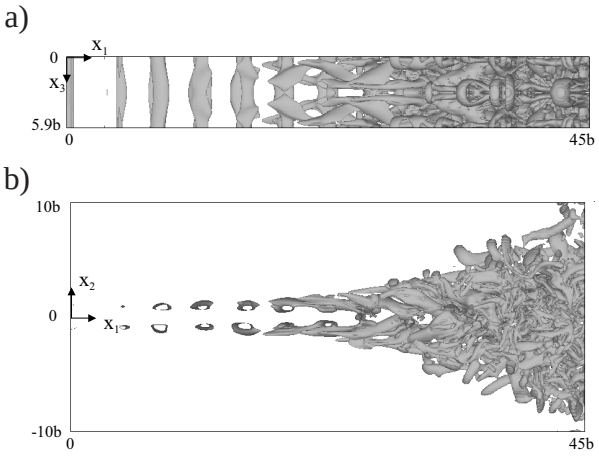

Fig. 2 Downstream evolution of second invariant Q structure (iso-surfaces of $Q = 0.1$) for 0.5% eigenfunction case (E1); a) topview and b) seideview.

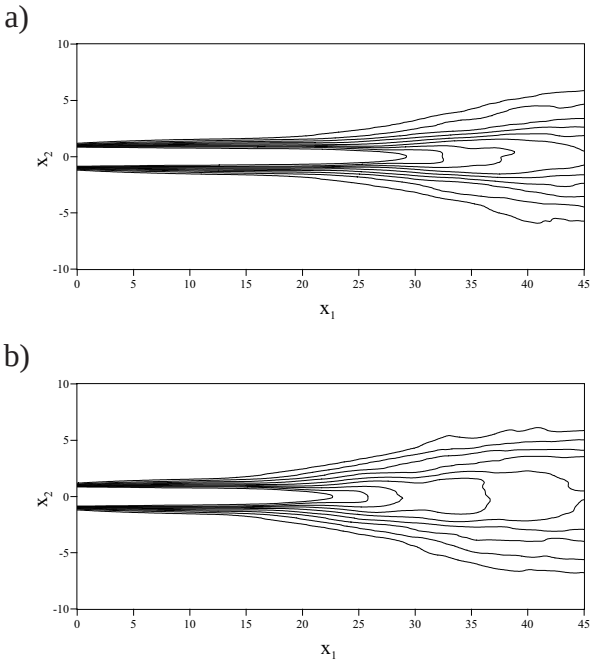

Fig. 3 Downstream evolution of mean streamwise velocity (contour plots); a) 0.5% eigenfunction case (E1) and b) 1% eigenfunction case (E2).

shaped structures appear.

The centerline streamwise velocity shown in figure 4 clearly indicates the location where the potential core closes. This figure also shows the result of the jet flow perturbed with only 3-D A1 modes, as shown by dotted lines in Fig.4. Increase of the amplitude level of the 3-D A1 mode leads to the sooner upstream core collapsing.

A comparison of the E2 case and the only 1% 3-D A1 modes E1 case suggests one that there is the same point of potential core collapsing. Consequently, the disappearance of potential core and the spread of the jet shear layer are dominated by the 3-D A1 modes, while the effects of the 2-D modes are small.

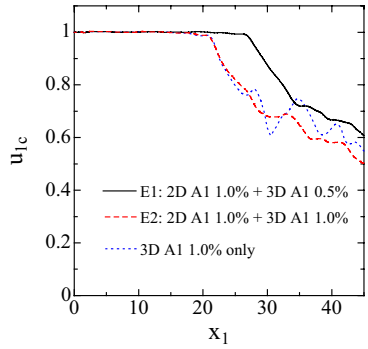

Fig. 4 Mean jet centerline velocity u_{1c}

For understanding of the effects of the different forcing, eigenfunction case (E1 case) and random disturbance (R2 case), the structure is visualized by iso-surface of Q and contours of mean streamwise velocity are shown in figure 5. For R2 case (figure 5(b)), many longitudinal vortex structures are formed in the jet forced with random disturbances.

The Λ-shaped structures appear clearly for E1 case, but not for R2 case. For R2 case, downstream of $x_1 < 20b$, the expansions of the jet share layers are slightly and earlier compared to E1 case. It seems to be caused by the earlier formation of longitudinal vortex structures for R2 case. Downstream of $x_1 > 20b$, the share layers hold the almost same expansion rate, while the share layers spread rapidly due to appearance of the Λ-shaped structures for E1 case. As seen in figure 6, the effects of the evolution of the vortex structures on the center line velocity variation is clear. The jet centerline velocity starts to decay around $x_1 = 20b$ and decreases slowly for R2 case. On the other hand, for E1 case, the center-

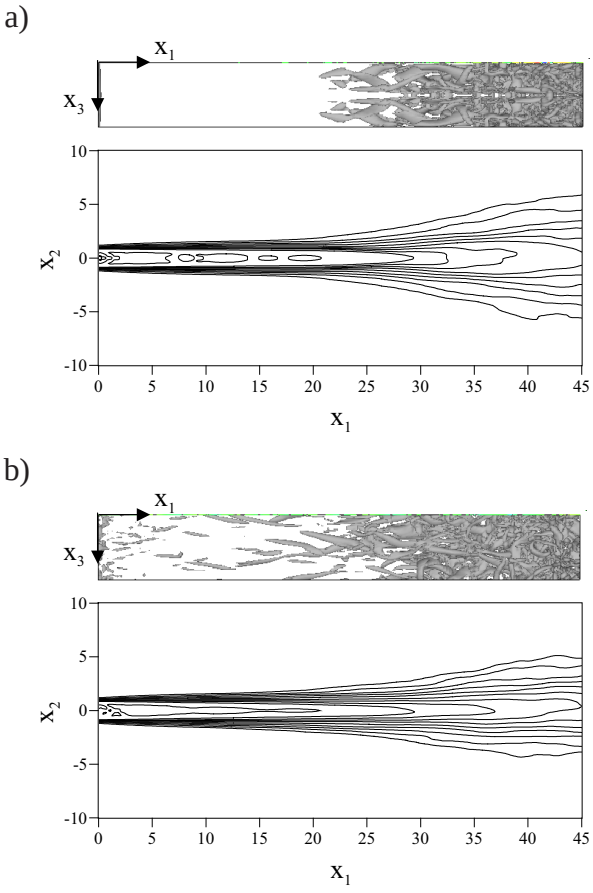

Fig. 5 Downstream evolution of second invariant Q structure (topview: iso-surfaces of $Q = 0.1$) and mean streamwise velocity (contour plots); a) 0.5% eigenfunction case (E1) and b) 3% random case (R2).

line velocity decreases rapidly around $x_1 = 27b$. As stated above, this rapid decrease is caused by the Λ-shaped structures. This rapidly decrease appears at the locations of $27b < x_1 < 32b$, and downstream at $x_1 > 32b$, the decrease rate becomes almost the same as R2 case. The location of the end of potential core depends on the inflow disturbance, such as the magnitude. Freund, Lele & Moin (2000)[5] and Freund (2001)[10] reported those of the round jets were $10r_0$ for $M_j = 1.92$, $Re_D = 2000$ and $12r_0$ for $M_j = 0.9$, $Re_D = 3600$, respectively. Note that the effect of the inflow disturbance is very important for downstream evolutions of the supersonic jet.

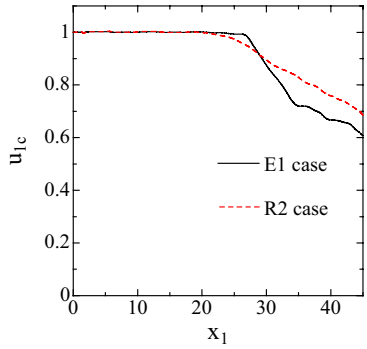

Fig. 6 Mean jet centerline velocity u_{1c}

3.2 Acoustic field

As seen in figure 6, for E1 and R2 cases, the locations where the potential core collapses are almost the same. In figure 7, the pressure fluctuations at the z=0 plane are visualized with vortical structures for the two cases. As shown in figure 7(a), for E1 case, the growth of the 2-D A1 mode makes the antisymmetric pressure fluctuation fields outside the jet, which are clearly observed up to the downstream locations of $x_1 < 30b$. In the same locations, the 2-D S2 mode generates the pressure waves confined primarily inside the jet. Pressure waves generated by these modes are amplified downstream up to the end of the jet potential core. Downstream after the appearance of the developed three-dimensional structures inside the jet, the effects of forced modes on pressure fields such as steep Mach waves are not clear outside the jet for the spatial simulations due to the narrow computational box in the vertical direction, which are observed in our temporally DNS.

For R2 case, due to the random inflow disturbances, many weak compression waves appear from the jet inflow plane and all of the week waves radiate at larger angles than that of A1 2-D mode, as shown in E1 case. Steep compression waves of the longer wavelength are observed downstream, which seem to radiate away from the jet at narrower angles to the jet axis. These observations suggest that a part of the higher wavenumber disturbances appear

first without enough growth and then the disturbances of higher growth rates develop downstream. These broadband supersonic phase disturbances lead to noise radiation.

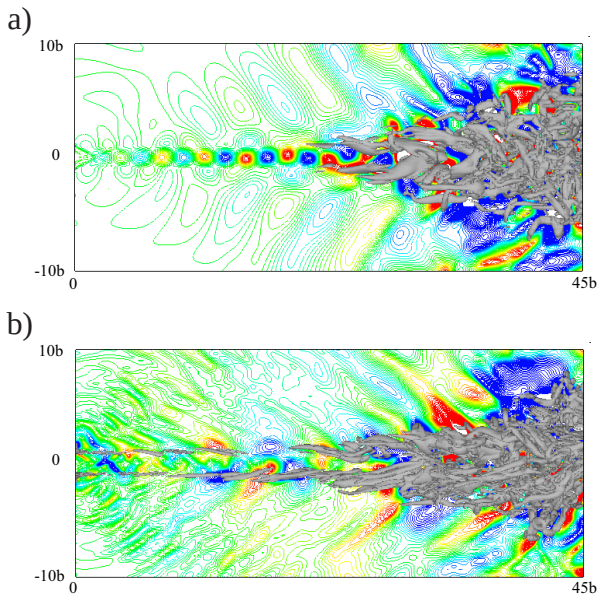

Fig. 7 Downstream evolution of second invariant Q structure (iso-surfaces of $Q = 0.1$) and pressure field (contour plots); a) 0.5% eigenfunction case (E1) and b) 3% random case (R2).

Figures 8 and 9 show the sound pressure levels (SPL) in the near acoustic field. As shown in figure 8(a) and figure 8(b) for E1 and R2 cases respectively, the acoustic radiation is highly directional. These figures indicate that the inflow disturbances affect the sound radiation field. For E1 case, as seen in the upstream regions, SPL profiles are dominated by the growth of acoustic components of the 2D-A1 mode traveling at supersonic speed along the jet axis. For R2 case, two kinds of sound radiation mechanism are visualized in the inlet and downstream regions. Near the inlet region, the non-equilibrium components in random inflow disturbances are emitted toward the jet outside. Further downstream, Mach waves at large angles are emitted due to the amplification of the 2-D A1 mode that has a short wave length and a high phase velocity, which is selectively amplified in the jet flow. Figure 9 of the cross-sectional profile of SPL shows that R1 case is slightly larger than E1 case outside the jet, though the SPL levels for E1 case is higher than R2 case inside the jet. However, these SPL results may be influenced by the small computational domain in the vertical direction.

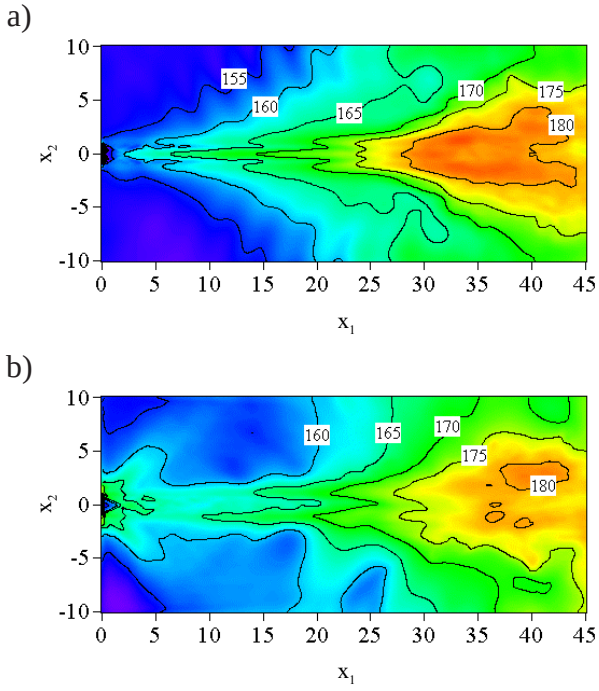

Fig. 8 Sound pressure levels in decibels for a) 0.5% eigenfunction case (E1) and b) 3% random case (R2).

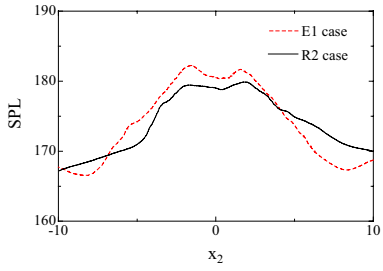

Fig. 9 Profiles of sound pressure levels in decibels at $x_1 = 35$.

Finally, numerical results of E1 case with a larger computational domain are presented. In this case, a computational grid is $N_{x_1} \times N_{x_2} \times N_{x_3} = 401 \times 301 \times 100$ and the computational regions are $0 < x_1 < 60b$, $-20b < x_2 < 20b$ and $0 <$

$L_3 < 2\pi/\beta\ b$, respectively. Figure 10 shows the iso-surfaces and the contours of the dilatation of div **u**. The radiating Mach waves have largely 2-D structures outside the jet, as seen in the acoustic far fields, but the near acoustic fields affected by the growth of the oblique modes are three-dimensional. Note that intense acoustic waves of div **u** radiate away from the downstream location where the jet core has collapsed. A comparison of figures 5(a) and 10 shows that the Mach waves emanate from the end of the potential core. These observations of noise radiation are very close to the sound fields found in Mach 1.92 round jets [3].

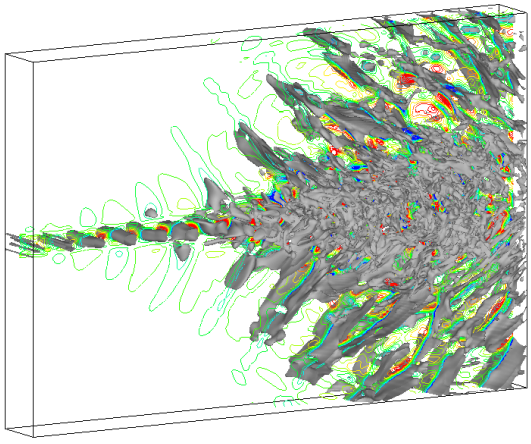

Fig. 10 Downstream evolution of dilatation field for 0.5% eigenfunction case (E1); iso-surfaces (div**u** $= 0.02$) and contour plots indicate the dilatation of div **u**.

4 Summary

Spatial DNS of a supersonic plane jet for $Mc = 1.17$ has been performed. The numerical results provide new physical insights into three-dimensional structures of a plane jet. Upstream disturbance conditions play an important role for the evolution of the downstream structure, such as development of shear layers and transition process in a jet. Growth of 3D-A1 mode is responsible for the Λ structure in a plane jet.

The 2-D A1 mode, whose phase velocity is larger than the ambient speed of sound, is responsible for the Mach waves emission. The growth and decay of the supersonic phase 2-D A1 mode link to the intense sound radiation in the 3D DNS.

Acknowledgments

Some of the simulations were executed at the Information Media Center of the Hiroshima University, the Information Technology Center of the University of Tokyo and Japan Aerospace Exploration Agency.

References

[1] Deng X, Maekawa H and Shen C. A Class of High Order Dissipative Compact Schemes. *AIAA Paper*, No. 96-1972, pp 1-11, 1996.

[2] Deng X, Maekawa H. Compact High Order Accurate Nonlinear Schemes. *J. Comput. Phys*, **130**, pp 77-91, 1997.

[3] Seiner J M. Fluid Dynamics and Noise Emission Associated with Supersonic Jets. *Studies in Turb.*, pp 297-323, 1992.

[4] Tam C K W. Supersonic Jet Noise. *Annu. Rev. of Fluid Mech.*, **27** pp 17-43, 1995.

[5] Freund J B, Lele S K and Moin P. Numerical Simulation of a Mach 1.92 Turbulent Jet and Its Sound Field. *AIAA J.*, **38**, 11, pp 2023-2039, 2000.

[6] Stanley S A, Sarkar S and Mellado J P. A study of the flow-field evolution and mixing in a planar turbulent jet using direct numerical simulation. *J. Fluid Mech.*, **450**, pp 377-407, 2002.

[7] Watanabe D and Maekawa H. Transition of Supersonic Plane Jet due to Symmetric/Antisymmetric Unstable Modes. *Journal of Turbulence*, **3**, 047, pp 1-17, 2002.

[8] Lele S K. Compact Finite Difference Schemes with Spectral-like Resolution. *J. Comput. Phys.*, **103**, pp 16-42, 1992.

[9] Poinsot T J and Lele S K. Boundary Conditions for Direct Simulations of Compressible Viscous Flows. *J. Comput. Phys.*, **101**, pp 104-128, 1992.

[10] Freund J B. Noise sources in a low-Reynolds-number turbulent jet at Mach 0.9. *J. Fluid Mech.*, **438**, pp 277-305, 2001.